

Articulate That Object Part (ATOP): 3D Part Articulation via Text and Motion Personalization

Aditya Vora¹ Sauradip Nag¹ Hao Zhang¹

¹Simon Fraser University, Canada



Figure 1. Given a textured mesh in rest state (left), the part to articulate (highlighted), and a text prompt as input, we first generate multi-view videos (middle) of plausible part articulation using our personalized diffusion model. We then transfer the motion from the generated videos back to the 3D mesh (right). The input meshes are the *top retrieval results* from Objaverse [8, 9] for “Trash can” and “Lamp.”

Abstract

We present ATOP (Articulate That Object Part), a novel few-shot method based on motion personalization to articulate a static 3D object with respect to a part and its motion as prescribed in a text prompt. Given the scarcity of available datasets with motion attribute annotations, existing methods struggle to generalize well in this task. In our work, the text input allows us to tap into the power of modern-day diffusion models to generate plausible motion samples for the right object category and part. In turn, the input 3D object provides image prompting to personalize the generated video to that very object we wish to articulate. Our method starts with a few-shot finetuning for category-specific motion generation, a key first step to compensate for the lack of articulation awareness by current diffusion models. For this, we finetune a pre-trained multi-view image generation model for controllable multi-view video genera-

tion, using a small collection of video samples obtained for the target object category. This is followed by motion video personalization that is realized by multi-view rendered images of the target 3D object. At last, we transfer the personalized video motion to the target 3D object via differentiable rendering to optimize part motion parameters by a score distillation sampling loss. Experimental results on PartNet-Sapient and ACD datasets show that our method is capable of generating realistic motion videos and predicting 3D motion parameters in a more accurate and generalizable way, compared to prior works in the few-shot setting.

1. Introduction

Everyday objects in the 3D world we live in undergo various movements and articulations. The ability to model and reason about object articulations in 3D plays an important role in simulation, design, autonomous systems, as well as robotic vision and manipulation. Over the past ten

years, there has been a steady build-up of digital 3D assets, from ShapeNet [5] (3M models) in the early days, to efforts on improving the assets’ structure (e.g., PartNet [40] with 27K finely segmented models) and quality (e.g., Amazon Berkeley Objects (ABO) [6] with \sim 8K models), and to the latest and largest open-source repository Objaverse-XL [8] (10M+ models). However, very few, if any, of these models come with part motions. Predominantly, they were all constructed in their rest (i.e., unarticulated) states. To our knowledge, the largest 3D datasets with part articulations, PartNet-Mobility [65] and Shape2Motion [60], only contain 2,346 and 2,440 *manually* annotated synthetic models, respectively. Clearly, human annotations are expensive in terms of time, cost, and expertise — they are not scalable to endow large volumes of 3D assets with articulations.

In this paper, we wish to develop a learning method to generate *plausible* and *accurate* articulations for *any* given 3D object, *without* relying on any human-annotated 3D part motions as most existing methods [1, 14, 16, 18, 41, 60, 67] do. In addition, we would also like to solve this problem in a *few-shot* setting, making the task even more challenging. Recently, there has been a surge of attempts to train foundational generative models for this task [30, 31]. However, the scarcity of annotated datasets significantly limits their generalization ability. With the recent success of *video diffusion models* [4, 12, 61, 66], it is natural to leverage their zero shot and open vocabulary capabilities to first generate motion videos for our target object and then perform a 2D-to-3D motion transfer. This approach is (3D) annotation-free, hence more scalable, but faces three key challenges to obtain accurate 3D part articulations:

- First, while SOTA video diffusion models can attain unprecedented visual quality for open-domain text-to-video generation, they are not yet well trained or sufficiently adaptive to generating articulations of everyday objects (e.g., even something as simple as a laptop), especially when typical *piecewise rigidity* is expected; see Fig. 2.
- Second, while current text-to-video models can generate plausible motions for *some* referenced object, to our knowledge, none of them can ensure that the generated motion is exactly of a *specific* (the target) 3D object.
- Third, current diffusion models still lack fine-grained control over which specific part should move.

To address these challenges, we present a novel method based on *motion personalization* to articulate a 3D object in the form of a mesh, with respect to a part prescribed in a *text prompt*; see Fig. 1. Our method is coined ATOP, for Articulate That Object Part, and it consists of three steps:

1. *Finetuning for category-specific motion video generation.* This is a key first step to compensate for the lack of articulation awareness by current video diffusion models. We finetune a pre-trained multi-view *image* generator, ImageDream [59], for *controllable multi-view video*

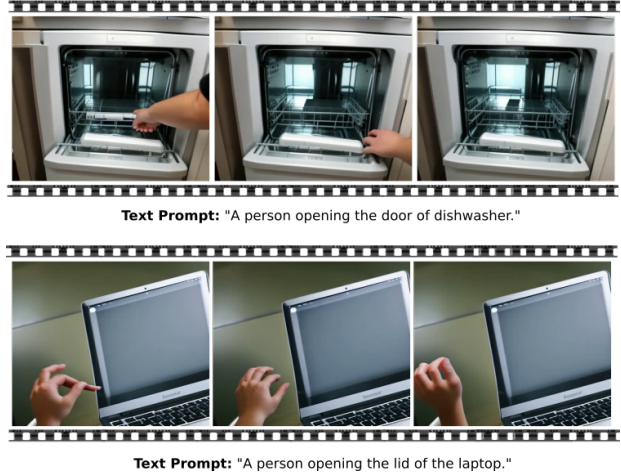


Figure 2. When prompted to generate object articulations, Stable Video Diffusion [4], a SOTA video diffusion model, cannot produce the desired part motion; only hand motions were observed.

generation, using *few-shot* video samples obtained for the target object category, that are of different objects from the target. We start from the pre-trained weights of ImageDream and inflate them for video processing, with motion region-of-interest and multi-view controls enabled through text and camera pose conditioning.

2. *Motion video personalization.* We render multi-view images and masks of the part which is to be articulated, for the target 3D mesh. These images, rendered masks, camera poses, and text prompt embeddings are fed to our diffusion model, which *hallucinates the desired part motion* from multi-views, personalized to the target object.
3. *Video-to-mesh motion transfer.* Using the personalized output from above, we transfer the plausible video motion to the target 3D object via differentiable rendering, which optimizes the motion axis parameters associated with the prescribed part by a score distillation sample (SDS) loss [45]; see Fig. 3 for an overview.

To our knowledge, ATOP presents the first annotation-free learning framework for generating accurate part articulations of existing 3D objects from text prompts. We present both qualitative and quantitative experiments to show that our method is not only capable of generating realistic personalized motion videos on unseen shapes, but also transferring the motion to 3D meshes, resulting in more accurate articulations in 3D than prior works in a few-shot setting.

2. Related Work

Mobility analysis. Understanding part mobility is essential for kinematics [1, 41]. Recent data-driven approaches leverage 3D datasets with articulation annotations to predict motion attributes. ScrewNet [16] infers articulations directly from depth image sequences without requiring part segmen-

tation, while Hu et al. [14] classify motion types from point clouds. Similarly, Shape2Motion [60], RPM-Net [67], and OPD [18] jointly predict motion-oriented part segmentation and attributes from point clouds and images. While these approaches enable fast inference, their reliance on extensive human annotations limits scalability and generalizability. In contrast, our method piggybacks on the knowledge of video foundational models to generalize under a few-shot setting.

Another line of works estimates motion attributes of an object as a by-product in the process of reconstructing digital twins of a scanned object [19, 32, 37, 52, 62]. However, different from our work, these methods focus on high fidelity reconstruction of the scanned object from multi-view images, monocular videos or depth maps where the scan is captured in different articulation states assuming the object is already articulated. In contrast to these approaches, our work focuses on estimating plausible motion axis parameters for a *static mesh*, hence enabling dynamic attributes.

Motion personalization. Diffusion models [13, 53, 54] have garnered significant interest for their training stability and remarkable performance in text-to-image (T2I) generation [3, 48]. Video generation [27, 36, 68] extends image generation to sequential frames, incorporating temporal dynamics. Recent advances [2, 11, 43, 51, 72] adapt T2I diffusion to spatio-temporal domains via architectural modifications. Personalizing motions using reference videos has gained traction, with methods such as Tune-a-Video [63] enabling one-shot video editing with structural control. Current approaches [17, 38] refine pre-trained text-to-video (T2V) models using regularization or frame residual losses, reducing dependency on training video appearances. Subject-driven video generation [42, 64, 71] finetunes video diffusion models but often struggles with overfitting and limited dynamics, failing to accurately capture 3D articulations. In contrast, our method proposes a motion personalization approach that enables controllable multi-view video generation, enabling part motions at desired spatial locations, which is crucial for articulation.

Generative articulation. With the rapid advancements in generative AI in recent years, the task of learning to represent, reconstruct, and generate object articulations from various input sources has become a prominent research area in visual computing [26, 31, 56]. NAP [28] employed diffusion models to synthesize articulated 3D objects by introducing a novel articulation graph parameterization. However, it faced limitations in scalability and controllability for articulations. CAGE [34] addressed these challenges by jointly modeling object parts and their motions within a graph-based structure. Recently, [33] proposed the seminal task of generating articulated objects from a single image. In contrast to these existing approaches that are focused on generating articulated assets, our goal is to enhance existing 3D assets by incorporating precise articulations.

Concurrent to our work, Articulate Any Mesh (AAM) [47] constructs a “digital twin” of an input 3D mesh with articulation, instead of directly inferring motion parameters on the input mesh as our work. For articulation generation, AAM leverages GPTo’s foundational knowledge on *joint classification* only, over the types of prismatic or revolute joints, while the joint locations and articulation axes are both estimated through heuristic shape analysis. With ATOP, we optimize motion axis directions by aligning them with plausible video outputs generated during the motion personalization step. This ensures that the target part is articulated correctly with proper motion axis orientations.

3. Method

3.1. Problem Setting

Given a small collection \mathcal{V} of multi-view (4 views) videos of articulated objects belonging to the same category (e.g., trashcans), along with a motion prompt τ (e.g., “The lid of the trash can is getting opened.”), our goal is to learn category-specific part motion and adapt and transfer the part motion into 3D space of a target mesh from the same shape category. To address this challenge, we decompose the problem into two main stages: *a) Motion Personalization* (Sec.3.2 and Sec.3.3) and *b) 3D Motion Axis Optimization* (Sec.3.4). In the first stage, the multi-view videos \mathcal{V} and the motion prompt τ are utilized to capture the dynamics of the object parts. This is achieved by finetuning a pre-trained image-to-multi-view diffusion (I2MV) model [59], enabling the synthesis of multi-view video data (Sec.3.2). Once trained, the fine-tuned model is then used to synthesize motion from multi-views for any target object from the same shape category (Sec.3.3). In the second stage (Sec.3.4), the synthesized multi-view videos are employed to extract the motion axis within 3D space, which subsequently guides the articulation of the 3D mesh \mathcal{M} . An overview of the problem formulation and the proposed methodology is depicted in Fig. 3.

3.2. Generating Multi-view Videos

As shown in Fig. 2, state-of-the-art diffusion models struggle with articulated motion. To address this, we introduce a finetuning step that efficiently incorporates multi-view articulation awareness into a diffusion model while preserving data efficiency and generalizability. This task is challenging because: (1) Existing finetuning methods for video generation [46, 63, 71] cannot generate 3D-aware, multi-view videos with generalizability. (2) Recent advances in 4D generation [29, 69] lack spatially controllable motion, which is essential for articulation. To overcome these limitations, we propose a finetuning strategy that adapts a multi-view image diffusion model [59] for controllable multi-view video generation. Since these models are image-

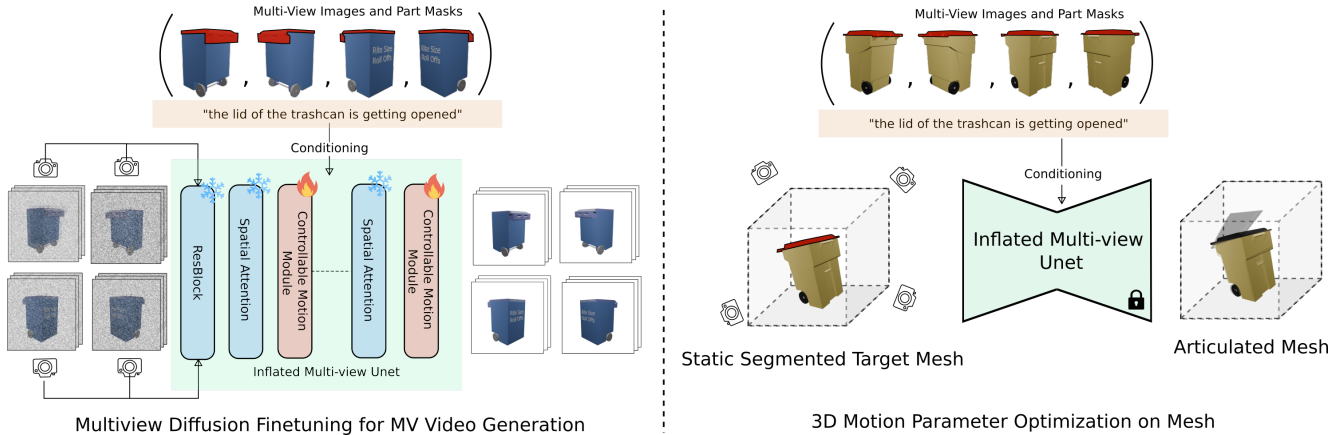


Figure 3. Pipeline Overview: Given a small collection of multi-view videos belonging to the same category our goal is to learn a category specific part motion by finetuning a multi-view image diffusion model. For this, noisy latents of the multi-view videos are denoised using the UNet blocks. Appearance information is injected into the UNet through conditioning, and controllability in part motion is achieved by injecting part masks into the diffusion process. Once finetuned, we can adapt the model for a new mesh and optimize the motion axis parameters with score distillation loss using the guidance of the diffusion model.

based, we extend them to videos using a network inflation approach [7, 63], enabling multi-view video synthesis.

Correspondence-Aware Spatial Attention. We want the generated multi-view videos to be geometrically consistent to ensure faithful reconstruction of coarse articulated shape during the 3D motion axis inference step.

For this, we inflate the correspondence aware self-attention module of ImageDream to capture the geometric consistency among the generated multi-view videos. Given a multi-view video as input during finetuning, we first encode these video frames into a $6D$ latent Z using a VAE encoder \mathcal{E} [25], and tokenize the latents to size $(B \times N_v \times N_f) \times (H \times W) \times F$ before applying self-attention using ImageDream’s pre-trained weights. Fig. 4 demonstrates how information is aggregated across views in the self-attention process. Because self-attention layers are trained to capture geometrical consistency across views, we reshape the tensors accordingly to apply attention across views at each frame index independently. This reshaping operation is given as:

$$Z_{out} = \text{reshape}(Z, (BN_v N_f)(HW)F \rightarrow (BN_f)(N_v HW)F) \quad (1)$$

Here, B is the batch size, N_v the number of views, N_f the number of frames, H and W the spatial dimensions, and F the feature dimension. The reshaped tensor Z_{out} is then used in subsequent layers. After the correspondence-aware spatial attention block, object appearance is integrated into the model via a cross-attention mechanism.

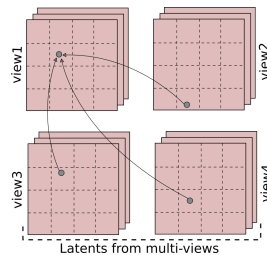


Figure 4. Correspondence-Aware Spatial Attention.

Cross Attention for Appearance Injection. Since our goal is to personalize the motion to the target shape, in addition to ensuring that the generated multi-view videos have geometric consistency, we also need to preserve the overall structure of the target shape across multiple views in the generated videos. This structural alignment helps produce pixel-accurate outputs that closely match the target mesh, ultimately improving the motion axis optimization during the motion inference step. For this, we leverage the pre-trained CLIP image encoder weights, which are trained along-with ImageDream diffusion model for incorporating images as an additional modality for 3D generation. To make sure that the object appearance is preserved across all the viewpoints, we provide multi-view conditioning through this CLIP Image encoder and fuse the information with the latents from the diffusion model. For this, *multiple views (e.g., 4) of the object’s rest state* are encoded into fixed-size embeddings using a pre-trained CLIP image encoder. These embeddings, along with CLIP text embeddings, are fused into the latent space via cross-attention, ensuring each view’s features align with its corresponding latent representation. This is achieved as follows:

$$F_{out} = \text{Attn}(Q, K_{txt}, V_{txt}) + \lambda \cdot \text{Attn}(Q, K_{img}, V_{img}) \quad (2)$$

In this setup, Q represents the query tokens from the latent Z , while K_{txt} and V_{txt} are the keys and values for the text embeddings. K_{img} and V_{img} are keys and values of image tokens. $\text{Attn}(\cdot)$ denotes the attention mechanism [57]. **Controllable Motion Module.** Besides geometric consistency and appearance injection, it is crucial for the diffusion model to learn the temporal motion patterns in the articulation videos. Improper temporal constraints would break the synchronization among different views and introduce geometric inconsistency. However, simply inserting a temporal

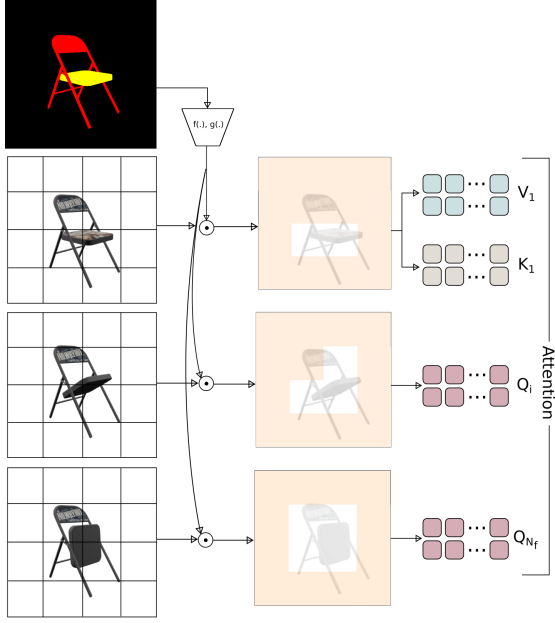


Figure 5. Controllable Motion Module. We modulate frame latents using an affine transformation predicted by blocks $f(\cdot)$ and $g(\cdot)$ from the binary mask. After this, attention is applied between the 1^{st} and n^{th} frames.

attention block within the diffusion model might not serve our purpose because our main goal is to achieve controllability in the motion generation so that the generated motion output can be spatially controlled using the part masks of the target object. To achieve this, we first add a new sparse spatio-temporal attention block that interpolates temporal features between the first and n^{th} frame using attention [57]. The latents Z from previous layers are then rearranged accordingly in order to apply temporal attention. This is given as:

$$Z_{out} = \text{reshape}(Z, (\text{BN}_f N_v)(\text{HW})F \rightarrow ((\text{BN}_v \text{HW})N_f F) \quad (3)$$

Next, in order to control the spatial location of the motion, we apply an *adaptive affine transformation* to the model’s intermediate features. For this, given a mask input \mathcal{B} and the mapping functions $f(\cdot)$ and $g(\cdot)$ we map the mask to scale γ and shift β and use them to modulate the latents as $Z' = \gamma \odot Z + \beta$. These functions are implemented using two-layer small convolutional blocks. A high-level overview of the controllable motion module is shown in Fig. 5. Temporal attention is then applied between the first and the last frames:

$$Z = \text{Attn}(Q_i, K_1, V_1) \quad (4)$$

Here, Q_i represents the query tokens of the i^{th} frame, while K_1 and V_1 are the keys and values from the first frame. The final output, Z , is then fed into the decoder VAE to generate the multi-view video.

Camera Controllability. For multi-view video generation, camera poses are incorporated into the diffusion model as a sequential input. They are first encoded using MLP layers, transforming them into pose embeddings. These embeddings are then fused with the timestep embeddings and added to the latents produced by the ResBlocks.

3.3. Personalized Motion Generation

In the previous section, we made design changes to the pre-trained multi-view image diffusion model with network inflation to adapt this model for multi-view video generation. We finetune this model using the few-shot training samples and update the newly added motion module. Post finetuning, we obtain a controllable multi-view video diffusion model, ψ^* . In order to generate personalized motion to a target mesh, we first render the 3D mesh in its rest state using the same fixed camera poses from finetuning. Then, given a text prompt (τ) and multi-view images \mathcal{I}_r , we infer the object’s motion from different views:

$$\hat{\mathcal{V}} = \psi^*(\mathcal{I}_r, \tau, \mathcal{B}) \quad (5)$$

Here, \mathcal{I}_r is the rendered image of the target mesh, and \mathcal{B} is the corresponding part segmentation mask. The generated personalized multi-view motion, $\hat{\mathcal{V}}$, is then used to estimate the 3D motion axis for the target mesh.

3.4. 3D Motion Axis Optimization

We leverage the personalized motion as a prior to robustly estimate the 3D motion parameters on a static target 3D mesh. Fig. 6 provides an overview of the 3D motion parameter optimization stage, which we detail below.

Estimating intermediate states: Given the input shape which is represented as a mesh \mathcal{M} , with vertices $\mathcal{V} \in \mathbb{R}^{n \times 3}$ and faces $\mathcal{F} \in \{1, 2, \dots, n\}^{m \times 3}$, we deform the mesh using the guidance from the personalized diffusion model. For this, we first parameterize the 3D representation for each frame of the video using N_g gaussians which are initialized with the points sampled from the input mesh. This representation is then optimized by distilling the category specific motion priors encapsulated in the personalized frozen diffusion model (ψ^*) using the score distillation loss Eq. 7. At each optimization step illustrated in Fig. 6 we use a differentiable renderer $\mathcal{R}(\cdot)$ [20, 21] to render multiple views of per-frame gaussians in 3D space to its corresponding frame in latent space of the diffusion model. The motion video rendered by these gaussians is then denoted as \mathcal{Z}_g . Next, we sample a diffusion timestep t and noise $\epsilon \sim \mathcal{N}(0, 1)$. We use this to add noise to the rendered latents and the noisy latents are then denoised using the personalized frozen diffusion model (ψ^*), where the diffusion model is conditioned using the text prompt, τ , rendered multi-view images \mathcal{I}_r and rendered segmentation masks \mathcal{B} of the target mesh. This optimization results in a sparse point cloud of the articulated shape for each time step.

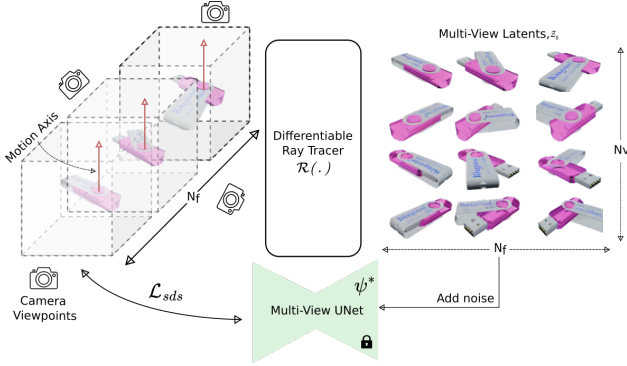


Figure 6. Approach of 3D motion axis optimization. We render the multi-view latent \mathcal{Z}_g using our differentiable renderer $\mathcal{R}(\cdot)$ and then optimize these latent using the guidance from our personalized motion model ψ^* .

Motion Axis Estimation: Given this sparse point cloud of intermediate articulated shape, our goal is to then estimate the motion attributes: *motion axis* and *motion origin*. We focus on piecewise rigid motions, specifically *revolute* and *prismatic* which are the most widely appearing motion types in nature [32, 47]. Having obtained a sparse point cloud of articulated shape for each time step, we can directly optimize the motion axis parameters using chamfer distance loss. However, to further improve the accuracy we propose an algorithmic approach for the same. In this step, given the static mesh \mathcal{M} , we sample points from the segmented part to be articulated and approximate it with an oriented bounding box (OBB). From the OBB parameters, we determine 7 possible axis origins—one centroid and the centers of its six side faces—and 6 possible axis directions, derived from its three principal components and their negations. The dynamic part is then transformed under a piecewise rigid assumption, and we select the best axis and origin by minimizing the chamfer distance with the articulated point cloud. See the supplementary for algorithmic details.

3.5. Training Objectives

We train our model in a two stage paradigm: (a) Finetuning for Motion Personalization and (b) 3D Motion Axis Optimization respectively.

Finetuning Stage. During finetuning, we keep the diffusion model frozen and train only the controllable motion module (Eq. 4). The network is optimized using the multi-view diffusion objective \mathcal{L}_{LDM} , defined as:

$$\mathcal{L}_{LDM} = \mathbb{E}_{z_t, \tau, \mathcal{I}_r, \mathcal{B}, \mathcal{C}, \epsilon, t} [\|\epsilon - \epsilon_\theta(z_t; \tau, \mathcal{I}_r, \mathcal{B}, \mathcal{C}, t)\|^2]. \quad (6)$$

where, z_t represents the latents at time step t , τ is the text prompt, \mathcal{I}_r is the reference image, \mathcal{B} is the binary mask, and \mathcal{C} denotes the camera poses.

3D Motion Parameter Optimization. During 3D motion parameter optimization, we optimize the gaussians using SDS loss [45]. Since our generation is conditioned on

multi-view images \mathcal{I}_r and masks \mathcal{B} , the loss is defined as:

$$\nabla_{\theta} \mathcal{L}_{SDS} = \mathbb{E}_{t, \epsilon} \left[\omega(t) (\epsilon_\phi(z_{gt}; t, \tau, \mathcal{I}_r, \mathcal{B}) - \epsilon) \frac{\partial z_{gt}}{\partial \theta} \right] \quad (7)$$

Here, θ represents the parameters of the differentiable renderer $\mathcal{R}(\cdot)$, ϵ_ϕ is the UNet of the personalized diffusion model ψ^* , and z_{gt} is the latent rendered by the renderer with noise for timestep t . τ , \mathcal{I}_r , and \mathcal{B} refer to the text prompt, rendered image, and segmentation mask of the target mesh, respectively.

4. Experiments

In this section, we present the qualitative and quantitative results of our method’s ability to infer 3D motion parameters given only a static segmented mesh as input. Along with it we also compare our multi-view video outputs with other baselines.

4.1. Dataset and Metrics Details

We evaluate our approach using the PartNet-Mobility dataset [65], following the train-test split of [23, 35]. Each training shape is rendered into four view videos, capturing articulations like a folding chair’s seat movement. Views are set at azimuth angles of $[45^\circ, 135^\circ, 225^\circ, 315^\circ]$, with elevation at 10° for some categories and 30° for others. This views are fixed throughout our experiments. Each view consists of 10 frames at 256×256 resolution, along with first frame binary mask of the articulated part. To assess generalization, we perform *zero-shot* experiments on 135 objects from the ACD dataset [15] curated by [33], which includes challenging objects from ABO [6], 3D-Future [10], and HSSD [22]. This dataset provides textured segmented meshes with part annotations. We render multi-view images and segmentation masks using the same camera viewpoints.

We assess our approach in two steps: 1) Multi-View Video Generation and 2) 3D Motion Axis Parameter estimation. For temporal coherence, we use Frchet Video Distance (FVD) [55], while text alignment is measured with the CLIP score [39]. Spatial and temporal consistency are evaluated using PSNR and LPIPS [70]. To assess 3D motion axis parameter estimation, we follow [18, 60] and compute Mean Angular Error (MAE) and Mean Position Error (MPE) of the joint axis. MAE is the dot product between predicted and ground truth motion axes, while MPE is the euclidean distance between their joint origins.

4.2. Baselines & Result Discussions

Given the modules used in our approach, we assess the individual components of our pipeline by benchmarking them against appropriate baselines tailored to each step.

Multi-View Video Generation Baselines. Since no prior work directly predicts multi-view videos from *static multi-view images* in a *controllable manner*, we establish two

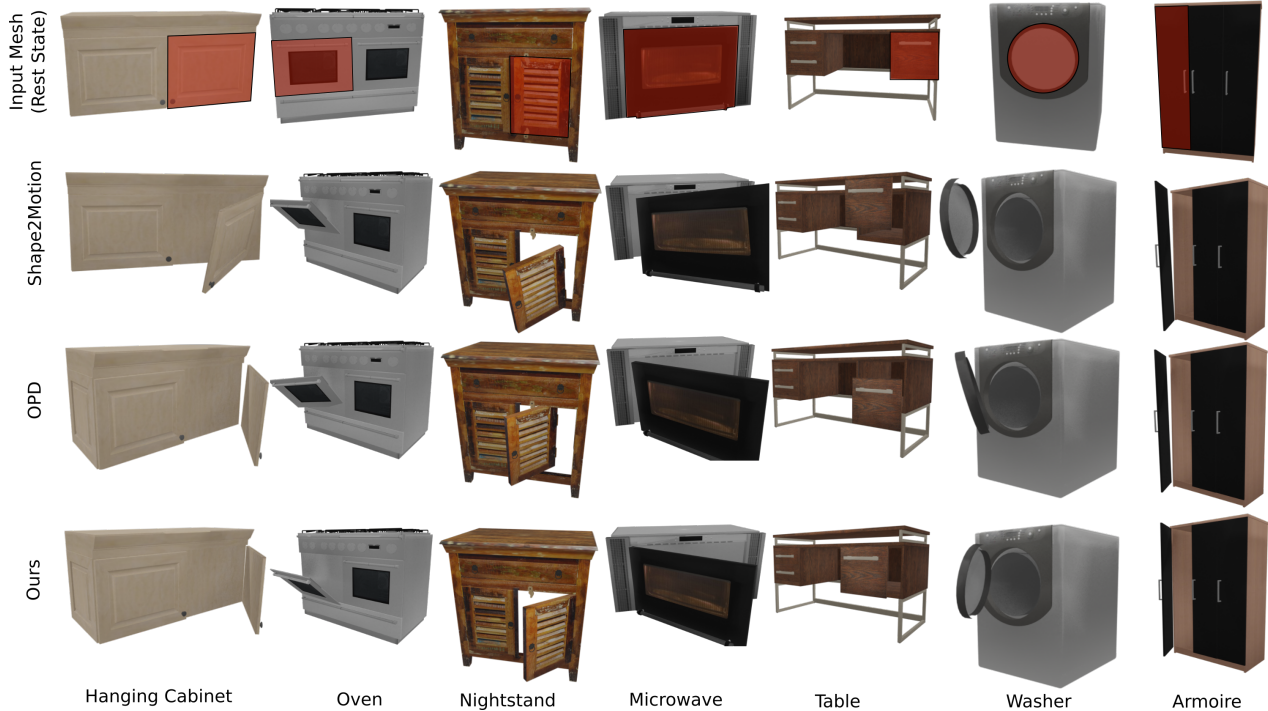


Figure 7. Qualitative results of part articulation on the ACD dataset [15]. The part to be articulated is highlighted in the first row. Note: The models in the ACD dataset do not have interiors.

baselines. The first baseline uses DynamiCrafter [66], where a pre-trained video diffusion model generates videos from multi-view images in a zero-shot manner. We denote this as MV+DC. The second baseline finetunes the ImageDream (ID[†]) [59] model without extra temporal attention. **3D Motion Axis Parameter Estimation Baselines.** Our pipeline estimates 3D motion axis parameters from a static, segmented 3D mesh using motion outputs from the multi-view diffusion model. We benchmark this step against Shape2Motion (S2M) [60] and Openable Part Detection (OPD) [18]. Shape2Motion predicts motion parameters from a point cloud and is trained end-to-end with 3D ground truth. OPD, on the other hand, estimates motion parameters from a single image using an object detection backbone that predicts segmentation masks, motion type, and motion parameters. We compare all these models in a few-shot setting by retraining them with our train and test split.

Discussions. As shown in Table 1, Table 2, and Fig. 7, our method predicts plausible motion parameters without using 3D annotations, beating the prior state-of-the-art methods by a large margin especially in angular error metrics. Shape2Motion outperforms OPD (Table 1) since it leverages point clouds, whereas OPD relies on single-image inputs. However, Shape2Motion struggles on the generalization dataset (Table 2) due to limited generalization capability of the 3D backbone network in a few-shot setting. In contrast, our method generalizes well showcasing the effectiveness of our approach. Beyond 3D motion parameter

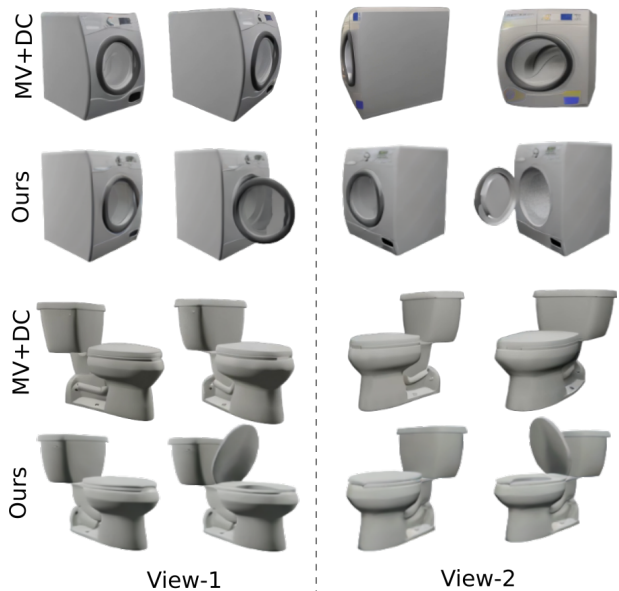


Figure 8. Qualitative comparison results of MV video generation.

estimation, we also compare our multi-view video generation results with the baselines. As shown in Table 3 and Fig. 8, our method outperforms the baselines in LPIPS, PSNR, and FVD, while achieving comparable CLIP scores. Fig. 8 highlights that MV+DC preserves the appearance of multi-view image inputs across all frames. However, it struggles with geometric consistency across views and has no articu-

Table 1. Quantitative results of Motion Parameter Estimation on PartNet-Mobility Dataset [65]

Metric	Method	Categories										
		Dish	Disp	Chair	Micro	Lamp	Oven	Fridge	Storage	Washer	Glasses	Mean
Ang Err ↓	S2M	8.93	4.21	8.33	3.82	9.76	7.97	5.44	5.28	6.58	10.12	7.04
	OPD	10.65	13.83	11.52	15.37	17.27	11.45	12.27	6.32	9.34	13.53	12.15
	Ours	1.95	0.83	5.77	1.14	3.64	1.36	1.77	1.65	3.81	4.47	2.63
Pos Err ↓	S2M	0.12	0.11	0.29	0.07	0.22	0.05	0.04	0.14	0.12	0.08	0.12
	OPD	0.21	0.17	0.36	0.09	0.18	0.08	0.08	0.12	0.11	0.16	0.15
	Ours	0.18	0.16	0.28	0.03	0.13	0.03	0.03	0.17	0.04	0.05	0.11

Table 2. Quantitative evaluation of zero-shot generalization on ACD dataset [15].

Metric	Method	Categories								Mean
		Armoire	Cabinet	NightStand	Table	Microwave	Oven	Refrigerator	Washer	
Ang Err ↓	S2M	17.32	19.34	22.37	21.62	23.56	22.56	25.42	19.77	21.49
	OPD	12.37	9.26	10.62	8.43	16.46	14.93	13.62	11.21	12.11
	Ours	2.83	3.29	3.92	2.39	3.52	3.34	2.96	6.75	3.63
Pos Err ↓	S2M	0.15	0.22	0.19	0.16	0.16	0.13	0.15	0.15	0.17
	OPD	0.22	0.25	0.19	0.21	0.25	0.27	0.19	0.18	0.22
	Ours	0.06	0.07	0.54	0.19	0.12	0.09	0.11	0.04	0.16

Method	CLIP (↑)	FVD (↓)	LPIPS (↓)	PSNR (↑)
MV+DC	25.51	1587.2	0.587	10.27
ID [†]	24.27	1258.4	0.373	13.79
Ours	24.89	963.9	0.132	20.06

Table 3. Quantitative evaluation of video generation

Table 4. **Ablation** Opt. vs. Algo.

Methods	Ag Er ↓	Ps Er ↓
Dir. Opt.	1.57	0.11
Algo. Opt.	0.98	0.07

Table 5. **Ablation** on # videos

# Vids	FVD ↓	PSNR ↑
1	1296.2	14.23
4	1172.3	17.78
8	983.7	19.83

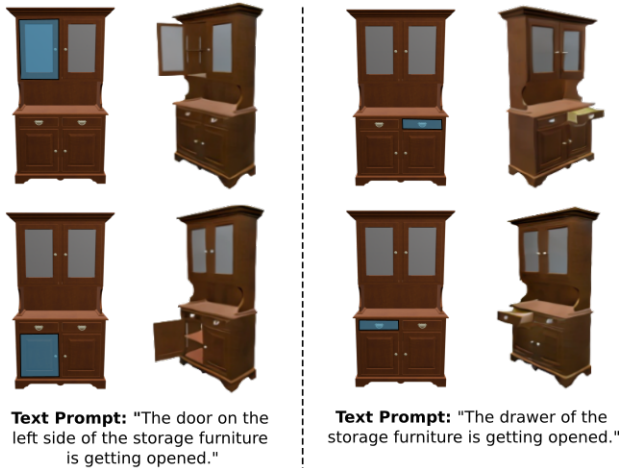


Figure 9. Effect of Masking in Articulation.

lation motion, reinforcing our claims in Sec. 1 and Fig. 2. In contrast, as can be seen in Fig. 8 and Table 3 our results achieves best PSNR, LPIPS and FVD scores which shows that our method is able to generate 3D consistent output along with successful articulation.

5. Ablations

In Table 4 and Table 5 and Fig. 9 we demonstrate the efficacy of several design choices. First, in Table 4 we show how our algorithm based optimization yields much better results compared to optimizing the motion axis parameters directly with chamfer distance loss. In Table 5 we show how the generation quality of multi-view videos is affected as we increase the number of videos for finetuning. As can be seen in Table 5 temporal consistency significantly falls as we reduce the number of videos. Finally in Fig. 9 we show the motion controllability of our method. As can be seen, by providing the appropriate part mask, we can control the spatial location of the part motion.

6. Conclusion, limitation, and future work

We introduce ATOP, the first method for adding realistic part articulation to existing 3D assets using text prompts and motion personalization. Unlike works such as [28, 34], which focus on generating articulated assets, our goal is to enhance static 3D models by inferring motion attributes. While ATOP achieves high accuracy in 3D part articulation, it has some limitations. First, our method currently supports only revolute and prismatic motions and does not handle multiple moving parts simultaneously, though it can infer different part motions in separate inference steps. Second, our model requires a segmented mesh as input, which can sometimes be a constraint. However, with recent advances in vision-language models (VLMs) [23, 35, 50], obtaining segmented meshes has become more accessible. By rendering multiple views of a mesh, VLMs can generate part segmentations, which can then be mapped back to the original mesh. In future, we will focus on expanding scalability across object categories and enabling cross-category motion

transfer—e.g., opening vehicle and room doors using few-shot learning from cabinet-opening videos. More broadly, our approach is a step toward animating vast existing 3D assets, but challenges like the “missing interior” problem remain, as most models lack interiors.

References

- [1] Ben Abbatematto, Stefanie Tellex, and George Konidaris. Learning to generalize kinematic models to novel objects. In *Proceedings of the 3rd Conference on Robot Learning*, 2019. 2
- [2] Amirhossein Alimohammadi, Sauradip Nag, Saeid Asgari Taghanaki, Andrea Tagliasacchi, Ghassan Hamarneh, and Ali Mahdavi Amiri. Smit: Segment me in time. *arXiv preprint arXiv:2410.18538*, 2024. 3
- [3] Yogesh Balaji, Seungjun Nah, Xun Huang, Arash Vahdat, Jiaming Song, Karsten Kreis, Miika Aittala, Timo Aila, Samuli Laine, Bryan Catanzaro, et al. ediffi: Text-to-image diffusion models with an ensemble of expert denoisers. *arXiv preprint arXiv:2211.01324*, 2022. 3
- [4] Andreas Blattmann, Tim Dockhorn, Sumith Kulal, Daniel Mendelevitch, Maciej Kilian, Dominik Lorenz, Yam Levi, Zion English, Vikram Voleti, Adam Letts, et al. Stable video diffusion: Scaling latent video diffusion models to large datasets. *arXiv preprint arXiv:2311.15127*, 2023. 2
- [5] Angel X Chang, Thomas Funkhouser, Leonidas Guibas, Pat Hanrahan, Qixing Huang, Zimo Li, Silvio Savarese, Manolis Savva, Shuran Song, Hao Su, Jianxiong Xiao, Li Yi, and Fisher Yu. ShapeNet: An information-rich 3D model repository. *arXiv preprint arXiv:1512.03012*, 2015. 2
- [6] Jasmine Collins, Shubham Goel, Kenan Deng, Achleshwar Luthra, Leon Xu, Erhan Gundogdu, Xi Zhang, Tomas F Yago Vicente, Thomas Dideriksen, Himanshu Arora, Matthieu Guillaumin, and Jitendra Malik. ABO: dataset and benchmarks for real-world 3D object understanding. In *CVPR*, pages 21126–21136, 2022. 2, 6
- [7] Yuren Cong, Mengmeng Xu, Christian Simon, Shoufa Chen, Jiawei Ren, Yanping Xie, Juan-Manuel Perez-Rua, Bodo Rosenhahn, Tao Xiang, and Sen He. Flatten: optical flow-guided attention for consistent text-to-video editing. 2024. 4
- [8] Matt Deitke, Ruoshi Liu, Matthew Wallingford, Huong Ngo, Oscar Michel, Aditya Kusupati, Alan Fan, Christian Laforte, Vikram Voleti, Samir Yitzhak Gadre, Eli VanderBilt, Anirudha Kembhavi, Carl Vondrick, Georgia Gkioxari, Kiana Ehsani, Ludwig Schmidt, and Ali Farhadi. Objaverse-xl: A universe of 10m+ 3d objects, 2023. 1, 2
- [9] Matt Deitke, Ruoshi Liu, Matthew Wallingford, Huong Ngo, Oscar Michel, Aditya Kusupati, Alan Fan, Christian Laforte, Vikram Voleti, Samir Yitzhak Gadre, et al. Objaverse-xl: A universe of 10m+ 3d objects. *Advances in Neural Information Processing Systems*, 36, 2024. 1
- [10] Huan Fu, Rongfei Jia, Lin Gao, Mingming Gong, Binqiang Zhao, Steve Maybank, and Dacheng Tao. 3d-future: 3d furniture shape with texture. *International Journal of Computer Vision*, 129:3313–3337, 2021. 6
- [11] Songwei Ge, Seungjun Nah, Guilin Liu, Tyler Poon, Andrew Tao, Bryan Catanzaro, David Jacobs, Jia-Bin Huang, Ming-Yu Liu, and Yogesh Balaji. Preserve your own correlation: A noise prior for video diffusion models. *arXiv preprint arXiv:2305.10474*, 2023. 3
- [12] Yuwei Guo, Ceyuan Yang, Anyi Rao, Zhengyang Liang, Yaohui Wang, Yu Qiao, Maneesh Agrawala, Dahua Lin, and Bo Dai. Animatediff: Animate your personalized text-to-image diffusion models without specific tuning. *arXiv preprint arXiv:2307.04725*, 2023. 2
- [13] Jonathan Ho, Ajay Jain, and Pieter Abbeel. Denoising diffusion probabilistic models. *Advances in neural information processing systems*, 33:6840–6851, 2020. 3
- [14] Ruizhen Hu, Wenchao Li, Oliver Van Kaick, Ariel Shamir, Hao Zhang, and Hui Huang. Learning to predict part mobility from a single static snapshot. *ACM Transactions On Graphics (TOG)*, 36(6):1–13, 2017. 2, 3
- [15] Denys Iliash, Hanxiao Jiang, Yiming Zhang, Manolis Savva, and Angel X Chang. S2o: Static to openable enhancement for articulated 3d objects. *arXiv preprint arXiv:2409.18896*, 2024. 6, 7, 8, 12, 15, 16
- [16] Ajinkya Jain, Rudolf Lioutikov, Caleb Chuck, and Scott Niekum. Screwnet: Category-independent articulation model estimation from depth images using screw theory. In *2021 IEEE International Conference on Robotics and Automation (ICRA)*, pages 13670–13677. IEEE, 2021. 2
- [17] Hyeonho Jeong, Geon Yeong Park, and Jong Chul Ye. Vmc: Video motion customization using temporal attention adaption for text-to-video diffusion models. *arXiv preprint arXiv:2312.00845*, 2023. 3
- [18] Hanxiao Jiang, Yongsen Mao, Manolis Savva, and Angel X Chang. Opd: Single-view 3d openable part detection. In *European Conference on Computer Vision*, pages 410–426. Springer, 2022. 2, 3, 6, 7
- [19] Zhenyu Jiang, Cheng-Chun Hsu, and Yuke Zhu. Ditto: Building digital twins of articulated objects from interaction. In *Proceedings of the IEEE/CVF Conference on Computer Vision and Pattern Recognition*, pages 5616–5626, 2022. 3
- [20] Leonid Keselman and Martial Hebert. Approximate differentiable rendering with algebraic surfaces. In *European Conference on Computer Vision*, pages 596–614. Springer, 2022. 5
- [21] Leonid Keselman and Martial Hebert. Flexible techniques for differentiable rendering with 3d gaussians. *arXiv preprint arXiv:2308.14737*, 2023. 5
- [22] Mukul Khanna, Yongsen Mao, Hanxiao Jiang, Sanjay Haresh, Brennan Shacklett, Dhruv Batra, Alexander Clegg, Eric Undersander, Angel X Chang, and Manolis Savva. Habitat synthetic scenes dataset (hssd-200): An analysis of 3d scene scale and realism tradeoffs for objectgoal navigation. In *Proceedings of the IEEE/CVF Conference on Computer Vision and Pattern Recognition*, pages 16384–16393, 2024. 6
- [23] Hyunjin Kim and Minhyuk Sung. Partstad: 2d-to-3d part segmentation task adaptation. In *European Conference on Computer Vision*, pages 422–439. Springer, 2024. 6, 8

- [24] Diederik P Kingma and Jimmy Ba. Adam: A method for stochastic optimization. *arXiv preprint arXiv:1412.6980*, 2014. 12
- [25] Diederik P Kingma and Max Welling. Auto-encoding variational bayes. *arXiv preprint arXiv:1312.6114*, 2013. 4
- [26] Long Le, Jason Xie, William Liang, Hung-Ju Wang, Yue Yang, Yecheng Jason Ma, Kyle Vedder, Arjun Krishna, Dinesh Jayaraman, and Eric Eaton. Articulate-anything: Automatic modeling of articulated objects via a vision-language foundation model. *arXiv preprint arXiv:2410.13882*, 2024. 3
- [27] Guillaume Le Moing, Jean Ponce, and Cordelia Schmid. Ccvs: context-aware controllable video synthesis. *Advances in Neural Information Processing Systems*, 34:14042–14055, 2021. 3
- [28] Jiahui Lei, Congyue Deng, William B Shen, Leonidas J Guibas, and Kostas Daniilidis. Nap: Neural 3d articulated object prior. *Advances in Neural Information Processing Systems*, 36:31878–31894, 2023. 3, 8
- [29] Bing Li, Cheng Zheng, Wenxuan Zhu, Jinjie Mai, Biao Zhang, Peter Wonka, and Bernard Ghanem. Vivid-zoo: Multi-view video generation with diffusion model. *Advances in Neural Information Processing Systems*, 37:62189–62222, 2024. 3
- [30] Ruining Li, Chuanxia Zheng, Christian Rupprecht, and Andrea Vedaldi. Dragapart: Learning a part-level motion prior for articulated objects. In *European Conference on Computer Vision*, pages 165–183. Springer, 2024. 2
- [31] Ruining Li, Chuanxia Zheng, Christian Rupprecht, and Andrea Vedaldi. Puppet-master: Scaling interactive video generation as a motion prior for part-level dynamics. *arXiv preprint arXiv:2408.04631*, 2024. 2, 3
- [32] Jiayi Liu, Ali Mahdavi-Amiri, and Manolis Savva. Paris: Part-level reconstruction and motion analysis for articulated objects. In *Proceedings of the IEEE/CVF International Conference on Computer Vision*, pages 352–363, 2023. 3, 6
- [33] Jiayi Liu, Denys Iliash, Angel X Chang, Manolis Savva, and Ali Mahdavi-Amiri. Singapo: Single image controlled generation of articulated parts in object. *arXiv preprint arXiv:2410.16499*, 2024. 3, 6
- [34] Jiayi Liu, Hou In Ivan Tam, Ali Mahdavi-Amiri, and Manolis Savva. Cage: Controllable articulation generation. In *Proceedings of the IEEE/CVF Conference on Computer Vision and Pattern Recognition*, pages 17880–17889, 2024. 3, 8
- [35] Minghua Liu, Yin hao Zhu, Hong Cai, Shizhong Han, Zhan Ling, Fatih Porikli, and Hao Su. Partslip: Low-shot part segmentation for 3d point clouds via pretrained image-language models. In *Proceedings of the IEEE/CVF Conference on Computer Vision and Pattern Recognition*, pages 21736–21746, 2023. 6, 8
- [36] Zhengxiong Luo, Dayou Chen, Yingya Zhang, Yan Huang, Liang Wang, Yujun Shen, Deli Zhao, Jingren Zhou, and Tieniu Tan. Videofusion: Decomposed diffusion models for high-quality video generation. In *Proceedings of the IEEE/CVF Conference on Computer Vision and Pattern Recognition*, pages 10209–10218, 2023. 3
- [37] Zhao Mandi, Yijia Weng, Dominik Bauer, and Shuran Song. Real2code: Reconstruct articulated objects via code generation. *arXiv preprint arXiv:2406.08474*, 2024. 3
- [38] Joanna Materzynska, Josef Sivic, Eli Shechtman, Antonio Torralba, Richard Zhang, and Bryan Russell. Customizing motion in text-to-video diffusion models. *arXiv preprint arXiv:2312.04966*, 2023. 3
- [39] Alexander H. Miller, Will Feng, Dhruva Tirumala, Adam Fisch, Augustus Odena, Vivek Ramavajjala, Joel Z. Leibo, Kelvin Guu and Jesse Engel, Jack Clark, Maruan H. Ali, Nazneen Rajani, Iain J. Dunning, Jacob Andreas, Chris Dyer, Dario Amodei, Jakob Uszkoreit, Douwe Pietsma, Tom Brown, and Ilya Sutskever. Clip: Learning to solve visual tasks by unsupervised learning of language representations. In *International Conference on Machine Learning*, 2020. 6
- [40] Kaichun Mo, Shilin Zhu, Angel X. Chang, Li Yi, Subarna Tripathi, Leonidas J. Guibas, and Hao Su. PartNet: A large-scale benchmark for fine-grained and hierarchical part-level 3D object understanding. In *The IEEE Conference on Computer Vision and Pattern Recognition (CVPR)*, 2019. 2
- [41] Kaichun Mo, Leonidas J Guibas, Mustafa Mukadam, Abhinav Gupta, and Shubham Tulsiani. Where2act: From pixels to actions for articulated 3d objects. In *Proceedings of the IEEE/CVF International Conference on Computer Vision*, pages 6813–6823, 2021. 2
- [42] Eyal Molad, Eliahu Horwitz, Dani Valevski, Alex Rav Acha, Yossi Matias, Yael Pritch, Yaniv Leviathan, and Yedid Hoshen. Dreamix: Video diffusion models are general video editors. *arXiv preprint arXiv:2302.01329*, 2023. 3
- [43] Sauradip Nag, Xi Tian Zhu, Jiankang Deng, Yi-Zhe Song, and Tao Xiang. DiffTad: Temporal action detection with proposal denoising diffusion. In *Proceedings of the IEEE/CVF International Conference on Computer Vision*, pages 10362–10374, 2023. 3
- [44] Adam Paszke, Sam Gross, Francisco Massa, Adam Lerer, James Bradbury, Gregory Chanan, Trevor Killeen, Zeming Lin, Natalia Gimelshein, Luca Antiga, et al. Pytorch: An imperative style, high-performance deep learning library. *Advances in neural information processing systems*, 32, 2019. 12
- [45] Ben Poole, Ajay Jain, Jonathan T. Barron, and Ben Mildenhall. Dreamfusion: Text-to-3d using 2d diffusion. *arXiv*, 2022. 2, 6
- [46] Chenyang Qi, Xiaodong Cun, Yong Zhang, Chenyang Lei, Xintao Wang, Ying Shan, and Qifeng Chen. Fatezero: Fusing attentions for zero-shot text-based video editing. In *Proceedings of the IEEE/CVF International Conference on Computer Vision*, pages 15932–15942, 2023. 3
- [47] Xiaowen Qiu, Jincheng Yang, Yian Wang, Zhehuan Chen, Yufei Wang, Tsun-Hsuan Wang, Zhou Xian, and Chuang Gan. Articulate anymesh: Open-vocabulary 3d articulated objects modeling. *arXiv preprint arXiv:2502.02590*, 2025. 3, 6
- [48] Aditya Ramesh, Mikhail Pavlov, Gabriel Goh, Scott Gray, Chelsea Voss, Alec Radford, Mark Chen, and Ilya Sutskever. Zero-shot text-to-image generation. In *International Conference on Machine Learning*, pages 8821–8831. PMLR, 2021. 3

- [49] Nikhila Ravi, Jeremy Reizenstein, David Novotny, Taylor Gordon, Wan-Yen Lo, Justin Johnson, and Georgia Gkioxari. Accelerating 3d deep learning with pytorch3d. *arXiv preprint arXiv:2007.08501*, 2020. 12
- [50] Nikhila Ravi, Valentin Gabeur, Yuan-Ting Hu, Ronghang Hu, Chaitanya Ryali, Tengyu Ma, Haitham Khedr, Roman Rädle, Chloe Rolland, Laura Gustafson, Eric Mintun, Junting Pan, Kalyan Vasudev Alwala, Nicolas Carion, Chao-Yuan Wu, Ross Girshick, Piotr Dollár, and Christoph Feichtenhofer. Sam 2: Segment anything in images and videos, 2024. 8
- [51] Uriel Singer, Adam Polyak, Thomas Hayes, Xi Yin, Jie An, Songyang Zhang, Qiyuan Hu, Harry Yang, Oron Ashual, Oran Gafni, et al. Make-a-video: Text-to-video generation without text-video data. *arXiv preprint arXiv:2209.14792*, 2022. 3
- [52] Chaoyue Song, Jiacheng Wei, Chuan Sheng Foo, Guosheng Lin, and Fayao Liu. Reacto: Reconstructing articulated objects from a single video. In *Proceedings of the IEEE/CVF Conference on Computer Vision and Pattern Recognition*, pages 5384–5395, 2024. 3
- [53] Jiaming Song, Chenlin Meng, and Stefano Ermon. Denoising diffusion implicit models. *arXiv preprint arXiv:2010.02502*, 2020. 3
- [54] Yang Song, Jascha Sohl-Dickstein, Diederik P Kingma, Abhishek Kumar, Stefano Ermon, and Ben Poole. Score-based generative modeling through stochastic differential equations. *arXiv preprint arXiv:2011.13456*, 2020. 3
- [55] Thomas Unterthiner, Sjoerd van Steenkiste, Karol Kurach, Raphaël Marinier, Marcin Michalski, and Sylvain Gelly. Fvd: A new metric for video generation. 2019. 6
- [56] Lukas Uzolas, Elmar Eisemann, and Petr Kellnhofer. Motiondreamer: Zero-shot 3d mesh animation from video diffusion models. *arXiv preprint arXiv:2405.20155*, 2024. 3
- [57] Ashish Vaswani, Noam Shazeer, Niki Parmar, Jakob Uszkoreit, Llion Jones, Aidan N Gomez, Lukasz Kaiser, and Illia Polosukhin. Attention is all you need. *Advances in neural information processing systems*, 30, 2017. 4, 5
- [58] Patrick von Platen, Suraj Patil, Anton Lozhkov, Pedro Cuenca, Nathan Lambert, Kashif Rasul, Mishig Davaadorj, Dhruv Nair, Sayak Paul, William Berman, Yiyi Xu, Steven Liu, and Thomas Wolf. Diffusers: State-of-the-art diffusion models. <https://github.com/huggingface/diffusers>, 2022. 12
- [59] Peng Wang and Yichun Shi. Imagedream: Image-prompt multi-view diffusion for 3d generation. *arXiv preprint arXiv:2312.02201*, 2023. 2, 3, 7
- [60] Xiaogang Wang, Bin Zhou, Yahao Shi, Xiaowu Chen, Qinpeng Zhao, and Kai Xu. Shape2motion: Joint analysis of motion parts and attributes from 3d shapes. In *Proceedings of the IEEE/CVF Conference on Computer Vision and Pattern Recognition*, pages 8876–8884, 2019. 2, 3, 6, 7
- [61] Xiang Wang, Hangjie Yuan, Shiwei Zhang, Dayou Chen, Junyi Wang, Yingya Zhang, Yujun Shen, Deli Zhao, and Jingren Zhou. Videocomposer: Compositional video synthesis with motion controllability. In *NeurIPS*, 2024. 2
- [62] Fangyin Wei, Rohan Chabra, Lingni Ma, Christoph Lassner, Michael Zollhoefer, Szymon Rusinkiewicz, Chris Sweeney, Richard Newcombe, and Mira Slavcheva. Self-supervised neural articulated shape and appearance models. In *Proceedings IEEE/CVF Conference on Computer Vision and Pattern Recognition (CVPR)*, 2022. 3
- [63] Jay Zhangjie Wu, Yixiao Ge, Xintao Wang, Stan Weixian Lei, Yuchao Gu, Wynne Hsu, Ying Shan, Xiaohu Qie, and Mike Zheng Shou. Tune-a-video: One-shot tuning of image diffusion models for text-to-video generation. *arXiv preprint arXiv:2212.11565*, 2022. 3, 4
- [64] Ruiqi Wu, Liangyu Chen, Tong Yang, Chunle Guo, Chongyi Li, and Xiangyu Zhang. Lamp: Learn a motion pattern for few-shot-based video generation. *arXiv preprint arXiv:2310.10769*, 2023. 3
- [65] Fanbo Xiang, Yuzhe Qin, Kaichun Mo, Yikuan Xia, Hao Zhu, Fangchen Liu, Minghua Liu, Hanxiao Jiang, Yifu Yuan, He Wang, et al. Sapien: A simulated part-based interactive environment. In *Proceedings of the IEEE/CVF conference on computer vision and pattern recognition*, pages 11097–11107, 2020. 2, 6, 8, 12
- [66] Jinbo Xing, Menghan Xia, Yong Zhang, Haoxin Chen, Wangbo Yu, Hanyuan Liu, Gongye Liu, Xintao Wang, Ying Shan, and Tien-Tsin Wong. Dynamicrafter: Animating open-domain images with video diffusion priors. In *European Conference on Computer Vision*, pages 399–417. Springer, 2024. 2, 7
- [67] Zihao Yan, Ruizhen Hu, Xingguang Yan, Luanmin Chen, Oliver Van Kaick, Hao Zhang, and Hui Huang. Rpm-net: recurrent prediction of motion and parts from point cloud. *arXiv preprint arXiv:2006.14865*, 2020. 2, 3
- [68] Lijun Yu, Yong Cheng, Kihyuk Sohn, José Lezama, Han Zhang, Huiwen Chang, Alexander G Hauptmann, Ming-Hsuan Yang, Yuan Hao, Irfan Essa, et al. Magvit: Masked generative video transformer. In *Proceedings of the IEEE/CVF Conference on Computer Vision and Pattern Recognition*, pages 10459–10469, 2023. 3
- [69] Haiyu Zhang, Xinyuan Chen, Yaohui Wang, Xihui Liu, Yunhong Wang, and Yu Qiao. 4diffusion: Multi-view video diffusion model for 4d generation. *Advances in Neural Information Processing Systems*, 37:15272–15295, 2024. 3
- [70] Richard Zhang, Phillip Isola, Alexei A Efros, Eli Shechtman, and Oliver Wang. The unreasonable effectiveness of deep features as a perceptual metric. In *CVPR*, 2018. 6
- [71] Rui Zhao, Yuchao Gu, Jay Zhangjie Wu, David Junhao Zhang, Jia-Wei Liu, Weijia Wu, Jussi Keppo, and Mike Zheng Shou. Motiondirector: Motion customization of text-to-video diffusion models. In *European Conference on Computer Vision*, pages 273–290. Springer, 2024. 3
- [72] Daquan Zhou, Weimin Wang, Hanshu Yan, Weiwei Lv, Yizhe Zhu, and Jiashi Feng. Magicvideo: Efficient video generation with latent diffusion models. *arXiv preprint arXiv:2211.11018*, 2022. 3

A. Implementation details

Our implementation is based on the Pytorch framework [44]. For diffusion, we use a popular library diffusers [58]. In both stages i.e. during finetuning as well as during 3D motion transfer stage we use Adam optimizer [24] to update the trainable parameters. During the finetuning stage, we set a learning rate of $5e^{-4}$, whereas during the 3D motion transfer stage, we set a learning rate of $5e^{-3}$. During finetuning, we train the model for 20000 iterations. A single multi-view video sample comprises of 4 views and 10 frames each. The resolution of each video is 256×256 . During the personalization step, we do inference for 50 steps using a classifier-free guidance scale of 5.0. Both finetuning and inference are done with fp16 model weights of ImageDream. During inference, we render the image using Blender, whereas the masks are rendered using Pytorch3D [49]. We finetune a single personalized diffusion model on Nvidia V100 GPU with 32Gb GPU memory. The training takes approximately 5hrs to complete. During inference, we sample 2048 points each on both static and dynamic part of the mesh and then initialize the gaussian centers with it. For our renderer, we set $\beta_1 = 21.4$, $\beta_2 = 2.66$. Because we optimize the points within the latent space of the diffusion model, we render features of resolution 32×32 .

B. Algorithm

Here, we explain in detail the algorithm used to retrieve the motion axis and origin from the point cloud. In this paper, we consider two types of motion, 1) Revolute Motion 2) Prismatic Motion.

Revolute Motion. Given a set of vertices of a mesh \mathcal{M} the revolute motion is represented as:

$$\vec{x}^* = \mathbf{R} (\vec{x} - \vec{o}) + \vec{o} \quad (8)$$

where, \vec{x} is the original mesh vertex, \vec{x}^* is the transformed mesh vertex after articulation, \vec{o} is motion axis origin, \mathbf{R} is the rotation matrix around the predicted motion axis direction, $\vec{a} = [a_x, a_y, a_z]$. Here, $\|\vec{a}\| = 1$. Given an angle θ , with which we want to rotate around the motion axis, we can compute the rotation matrix using Rodrigues formula as,

$$\mathbf{K} = \begin{bmatrix} 0 & -a_z & a_y \\ a_z & 0 & -a_x \\ -a_y & a_x & 0 \end{bmatrix}, \quad (9)$$

$$\mathbf{R} = \mathbf{I} + \sin(\theta) \mathbf{K} + (1 - \cos(\theta)) \mathbf{K}^2 \quad (10)$$

Prismatic Motion. Unlike revolute motion, prismatic motion is defined using only motion axis, \vec{a} , where $\|\vec{a}\| = 1$. Given a motion range $[M_{max}, M_{min}]$ within which we would like to articulate a part, the magnitude γ and ultimately the transformed vertex of the mesh \mathcal{M} is defined as:

$$\vec{a}^* = \gamma * \vec{a}, \quad \vec{x}^* = \vec{x} + \vec{a}^* \quad (11)$$

where, γ is the magnitude of scaling computed from the motion range, \vec{x} is the original mesh vertex and \vec{x}^* is the transformed mesh vertex. The algorithm to find motion parameters is described in Algorithm 1.

Algorithm 1: Find_Motion_Parameters()

input : Static Mesh \mathcal{M} , Point Clouds P_{N_f} , Motion Type M_{type} , Segmentation Labels L , Instance ID y

output: Motion Axis \vec{a} , Motion Origin \vec{o}

$\vec{a}, \vec{o} \leftarrow \vec{0}, \vec{0}$;

// Find *OBB*, where

$OBB = (\vec{v}_1, \vec{v}_2, \vec{v}_3, \vec{c}, d_{v_1}, d_{v_2}, d_{v_3})$

$OOB \leftarrow$

FindOrientedBoundingBox(\mathcal{M}, y);

$A_{hyp} \leftarrow (\vec{v}_1, \vec{v}_2, \vec{v}_3, -\vec{v}_1, -\vec{v}_2, -\vec{v}_3)$;

$O_{hyp} \leftarrow (\vec{c} \pm 0.5(d_{v_1} \cdot \vec{v}_1), \vec{c} \pm 0.5(d_{v_2} \cdot \vec{v}_2), \vec{c} \pm 0.5(d_{v_3} \cdot \vec{v}_3), \vec{c})$;

$min_dist \leftarrow 0.0$;

for each \vec{a}_i in A_{hyp} **do**

for each \vec{o}_i in O_{hyp} **do**

 // transform vertices of \mathcal{M} as per M_{type} & find best match.

if $M_{type} = \text{"revolute"}$ **then**

 Mesh $\mathcal{M}' \leftarrow \text{Revolute}(\mathcal{M}, \vec{a}_i, \vec{o}_i, y)$

 // Eq: 8

end

if $M_{type} = \text{"prismatic"}$ **then**

 Mesh $\mathcal{M}' \leftarrow \text{Prismatic}(\mathcal{M}, \vec{a}_i, y)$

 // Eq: 11

end

$P_{\mathcal{M}} \leftarrow \mathcal{M}.vertices$;

$e \leftarrow \text{chamfer_distance}(P_{\mathcal{M}}, P_{N_f})$;

if $e \leq min_dist$ **then**

$\vec{a} \leftarrow \vec{a}_i$; $\vec{o} \leftarrow \vec{o}_i$

end

end

end

C. Additional Results

We present additional results on PartNet Sapien Dataset [65]. The results are shown in Fig. 10. The part to be articulated is highlighted. As can be seen in the figure, our model is able to generalize within the same category of object of PartNet Sapien Dataset. In addition to this, we also show additional results of the generalization capability of our model on ACD dataset [15] i.e. the diffusion model is trained on PartNet Sapien dataset and tested on ACD dataset for generalization. As can be seen in Fig. 11 and Fig. 12 can generalize to unseen shapes over a different dataset. We

also show articulation results on the 3D mesh in the last column.

Input Mesh
(Rest State)



Display



Dishwasher



Lamp



Box



Bucket



FoldingChair



Eyeglasses



USB



Staplet

← Multi-View Videos →



Text Prompt: "the screen of the display is rotating around the hinge."



Text Prompt: "the door of the dishwasher with a hinge on the top is opening."



Text Prompt: "the lamp head is rotating."



Text Prompt: "the top lid of the box is opening."



Text Prompt: "the handle of the bucket is rotating."



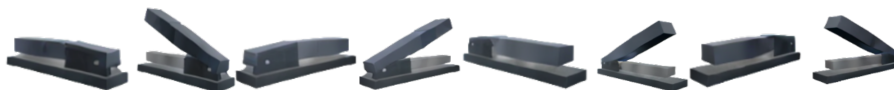
Text Prompt: "the chair seat is getting folded around the hinge."



Text Prompt: "the right temple of the eyeglasses is getting closed."



Text Prompt: "the usb lid is rotating around a joint."



Text Prompt: "the handle of the stapler is getting opened."

Articulated
Mesh



Figure 10. Qualitative results of Multi-View Video Generation and 3D motion axis prediction on PartNet Sapian Dataset.



Figure 11. Qualitative results of generalization of Multi-view video generation and 3D Motion Axis prediction on ACD dataset [15].



Figure 12. Qualitative results of generalization of Multi-view video generation and 3D Motion Axis prediction on ACD dataset [15].